Supplementary information

Facile Synthesis of Nitrogen-Doped Carbon Materials with Hierarchical Porous Structures for High-Performance Supercapacitors in Both Acid and Alkaline Electrolyte

Yuntong Li, Ling Liu, Yuzhe Wu, Tong Wu, Haiyang Wu, Qipeng Cai, Yiting Xu, Birong Zeng, Conghui Yuan* and Lizong Dai*

Fujian Provincial Key Laboratory of Fire Retardant Materials, College of Materials, Xiamen University, Xiamen, 361005, China.

E-mail: *yuanch@xmu.edu.cn, *lzdai@xmu.edu.cn

1. Characterization

^{1}H magnetic resonance (NMR) spectrum of the 2,4,6-Tris(4-aminophenyl)-1,3,5-triazine (**TAA**) was carried out on a Bruker Advanced II AV500 MHz NMR spectrometer. Fourier transform infrared spectoscopy (FT-IR) spectra was measured from a Nicolet Avatar 360. Scanning electron microscopy (SEM) images were taken using a Su-70 instrument. The X-ray photoelectron spectroscopy (XPS) spectra were tested on a PHI Quantum-2000 photoelectron spectrometer (Al Kα with 1486.6 eV). Electrochemical impedance spectroscopies (EIS) were carried out with the frequency of 10^{-2} to 10^5 Hz and at an amplitude of 5 mV.

2. Synthesis

Synthesis of TAA
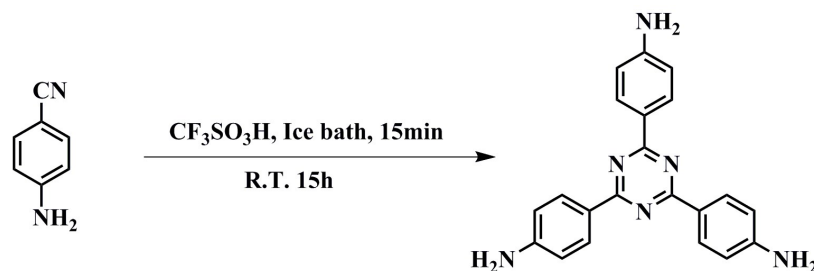
The synthesis of 2,4,6-tris(4-aminophenyl)-1,3,5-triazine (**TAA**) was performed according to previous literature procedure with a minor modification.[33] The detailed synthetic procedure and corresponding NMR are listed as follows:

0.708 g of 4-aminobenzonitrile (6 mmol) was added to 1 mL of trifluoromethane sulfonic acid in 10 mL round-bottom flask and stirred for 15 min at 0 °C by ice-bath. Then, the above mixed solution was further stirred for 15 h at room temperature. Subsequently, $NH_3 \cdot H_2O$ was added dropwise to the above solution to adjust pH value to 7. Finally, the resulting mixture was centrifuged for 3 times with large amount of deionized water and a yellow solid was obtained. [NMR] ^1H NMR (DMSO-d_6, 500 MHz) δ = 5.91 (s, 6H), 6.68 (d, 6H), 8.34 (d, 6H).

Synthesis of Aa-NCas
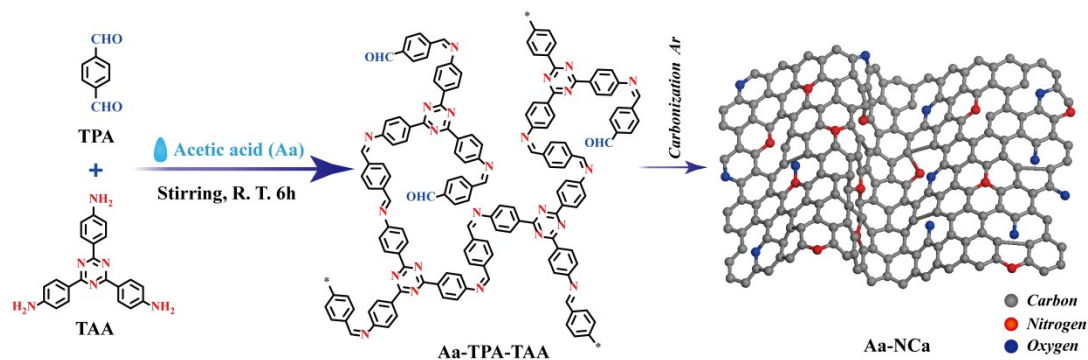
Scheme S1. Synthetic procedure of Aa-TPA-TAA and Aa-NCa by using acetic acid as catalyst.

Typically, 0.709 g of TAA (2 mmol) and 0.40 g of TPA (3 mmol) were taken in a 50 mL round bottom flask and dissolved in 10 mL of 1,3,5-trimethylbenzene, 1,4-dioxane mixed solvent (v : v = 1 : 4). To this solution, 1 mL of acetic acid (Aa) was added, and stirred at room temperature for 6 h. The reaction mixture was then centrifuged, washed with ethanol for 3 times to remove unreacted monomers, thus affording solid powder. After drying in vacuum, the as-prepared precursor (Aa-TPA-TAA) was carbonized at 850 °C for 2 h with a heating rate of 5 °C min^{-1} under Ar atmosphere to prepare Aa-NCa$_{850}$.

Synthesis of Ta-NCbs
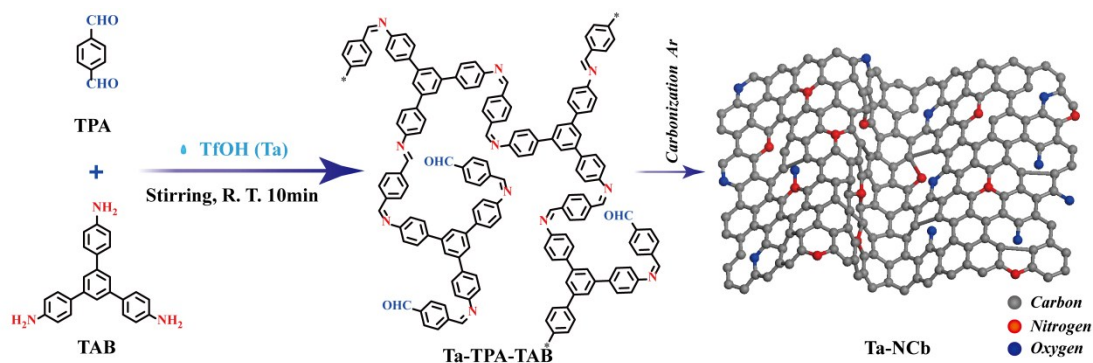
Scheme S2. Synthetic procedure of Ta-TPA-TAB and Ta-NCb by using TfOH as catalyst.

Typically, 0.702 g of 1,3,5-tris(4-aminophenyl)benzene (TAB) (2 mmol) and 0.40 g of TPA (3 mmol) were taken in a 50 mL round bottom flask and dissolved in 10 mL of 1,3,5-trimethylbenzene, 1,4-dioxane mixed solvent (v : v = 1 : 4). To this solution, 20 μL of trifluoromethanesulfonic acid was added, and precipitate was generated immediately. The reaction mixture was further stirred at room temperature for 10 min and then centrifuged, washed with ethanol for 3 times to remove unreacted monomers and afford solid powder. After drying in vacuum, the as-prepared precursor Ta-TPA-TAB was carbonized at 850 $^\circ$C for 2 h with a heating rate of 5 $^\circ$C min^{-1} under Ar atmosphere to prepare Ta-NCb$_{850}$.
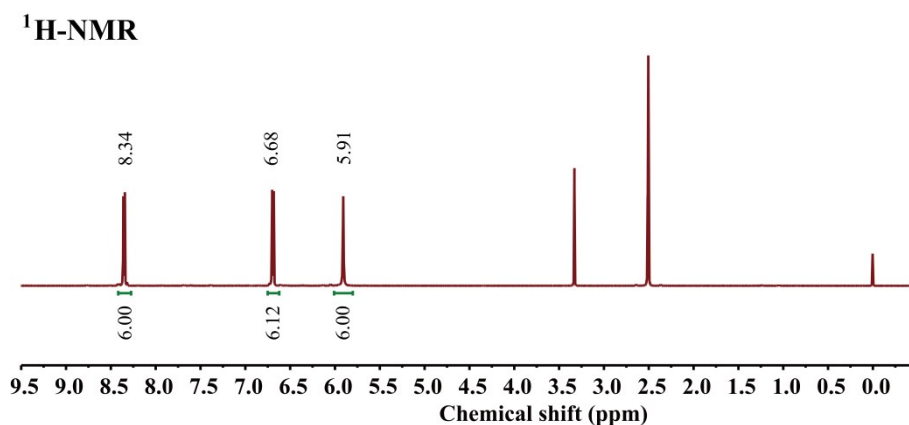
Fig. S1 ^{1}H spectrum of the TAA.
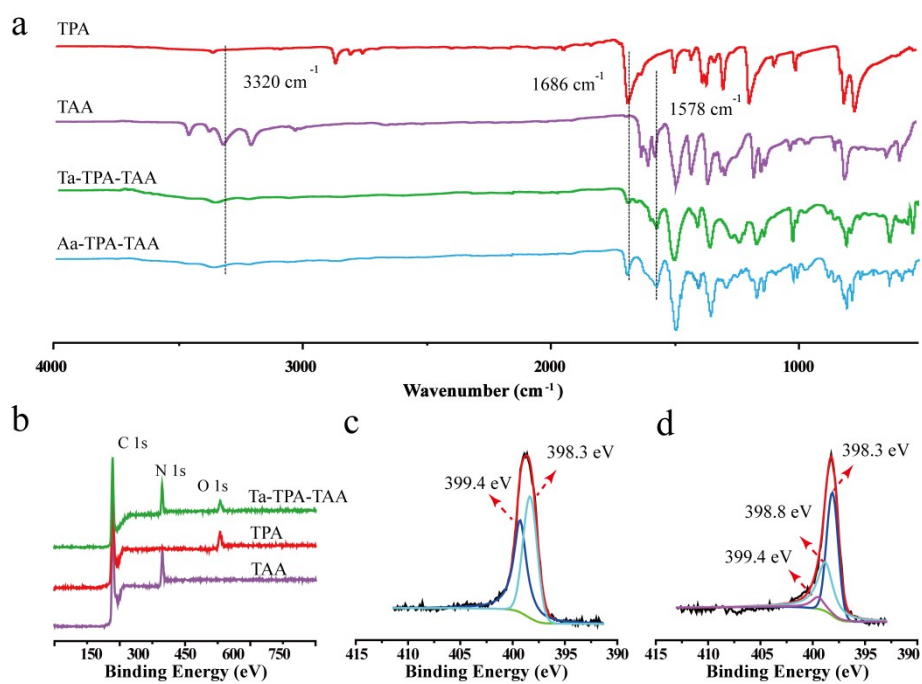
Fig. S2 FT-IR spectra of TPA, TAA, Ta-TPA-TAA and Aa-TPA-TAA (a); XPS survey spectra of TPA, TAA and Ta-TPA-TAA (b); High-resolution N 1s XPS spectra of TAA (c) and Ta-TPA-TAA (d).
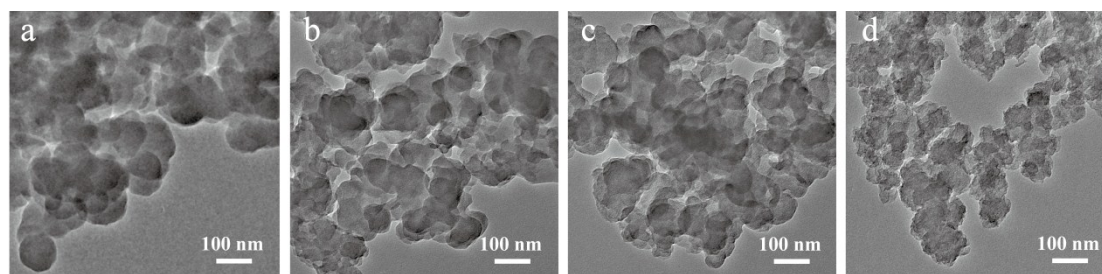
Fig. S3 TEM images of precursor Ta-TPA-TAA (a), Ta-NCa$_{650}$ (b), Ta-NCa$_{750}$ (c) and Ta-NCa$_{950}$ (d).
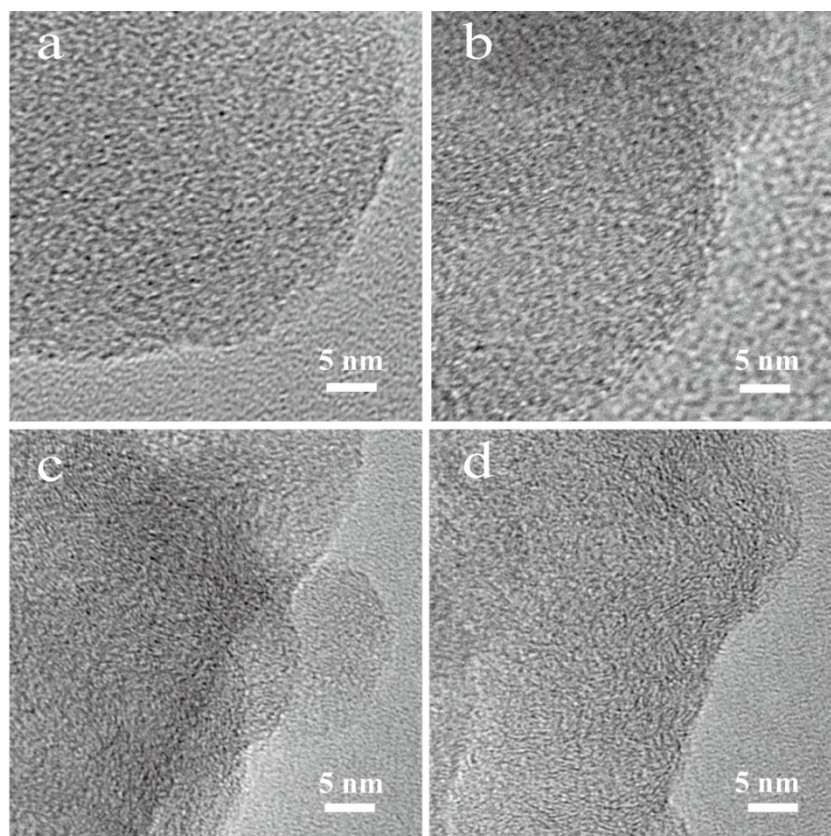
Fig. S4 High resolution TEM images of Ta-NCa$_{650}$ (a), Ta-NCa$_{750}$ (b), Ta-NCa$_{850}$ (c), Ta-NCa$_{950}$ (d).
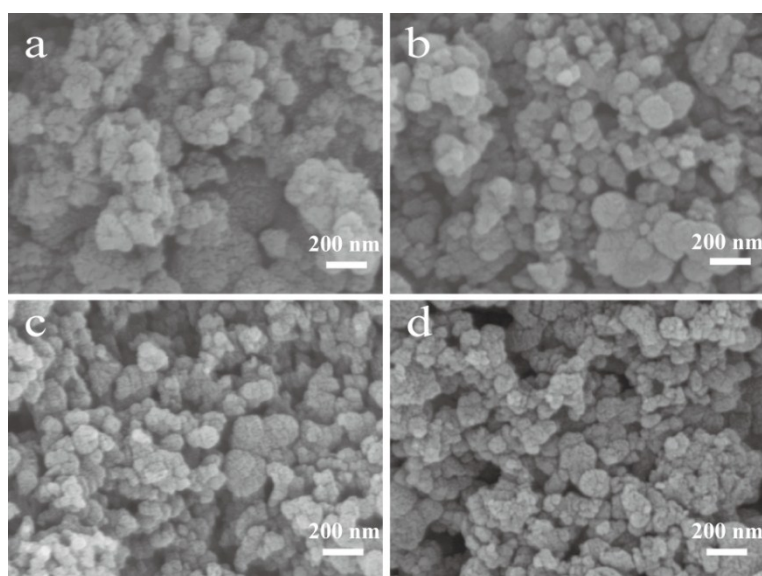
Fig. S5 SEM images of Ta-NCa$_{650}$ (a), Ta-NCa$_{750}$ (b), Ta-NCa$_{850}$ (c) and Ta-NCa$_{950}$ (d).
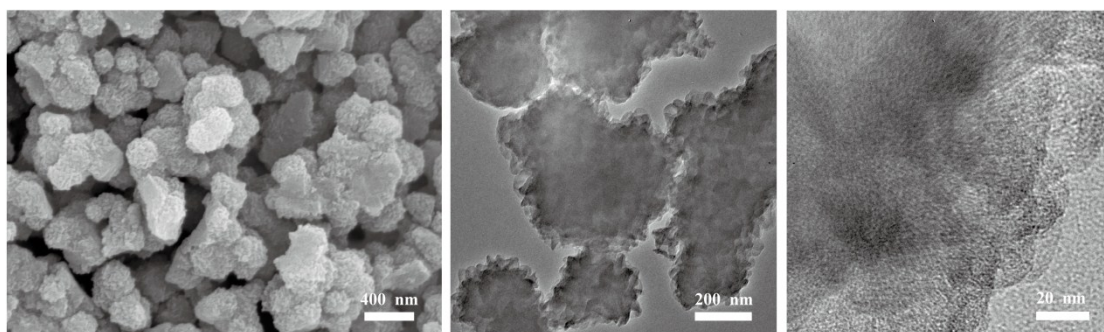
Fig. S6 SEM image of Aa-NCa$_{850}$ (a), TEM image of Aa-NCa$_{850}$ (b), high resolution TEM image of Aa-NCa$_{850}$ (c).
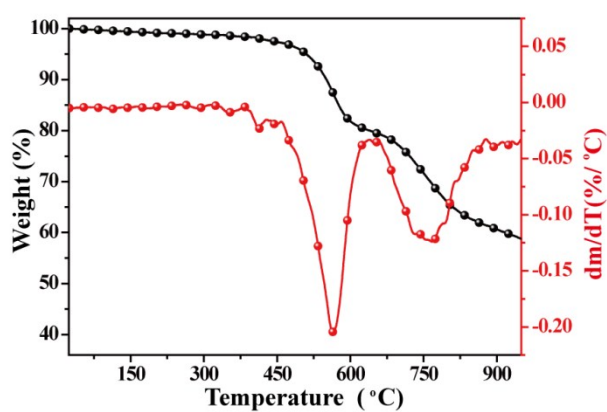
Fig. S7 TGA and DTA curves of precursor Ta-TPA-TAA.
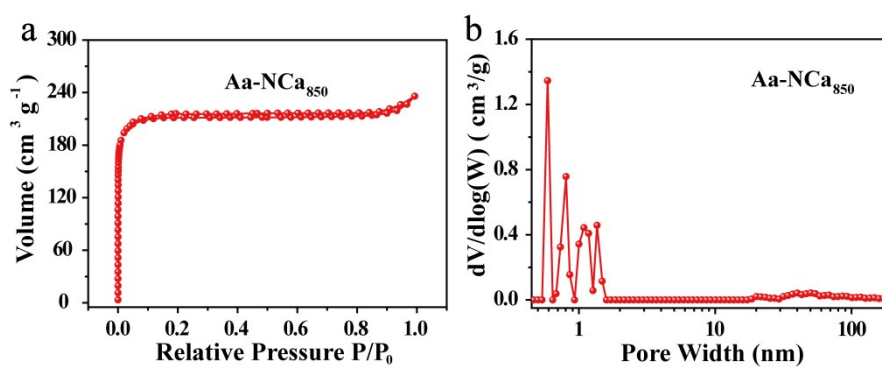
Fig. S8 N$_2$ adsorption/desorption isotherm (a) and the DFT pore size distribution (b) of Aa-NCa$_{850}$.
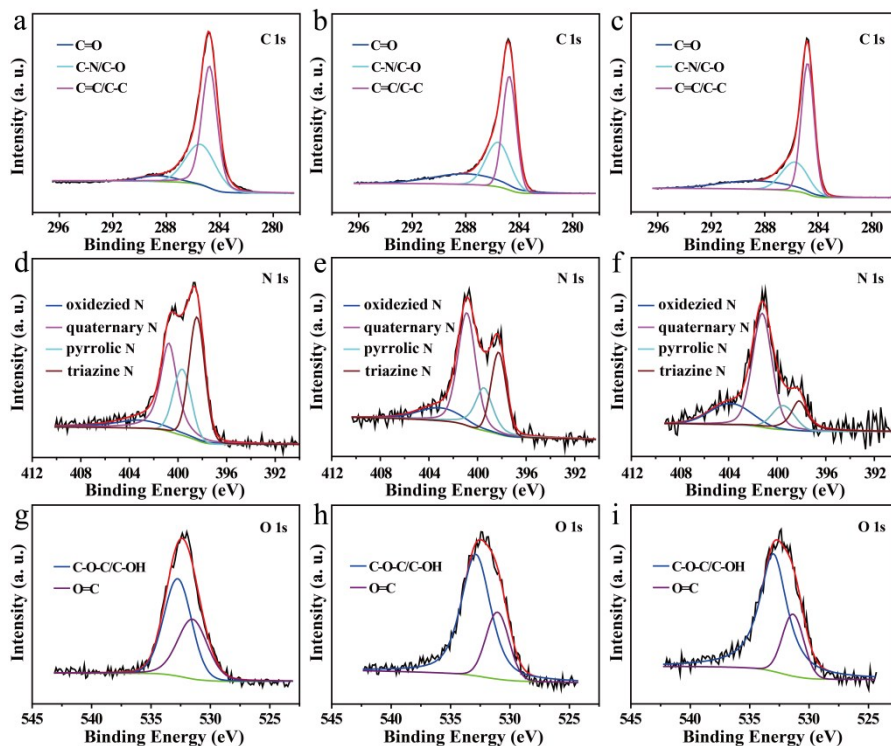
Fig. S9 High-resolution XPS spectra. Ta-NCa$_{650}$: of C 1s (a), N 1s (d) and O 1s (g) ; Ta-NCa$_{750}$: C 1s (b), N 1s (e) and O 1s (h); Ta-NCa$_{950}$: C 1s (c), N 1s (f) and O 1s (i).
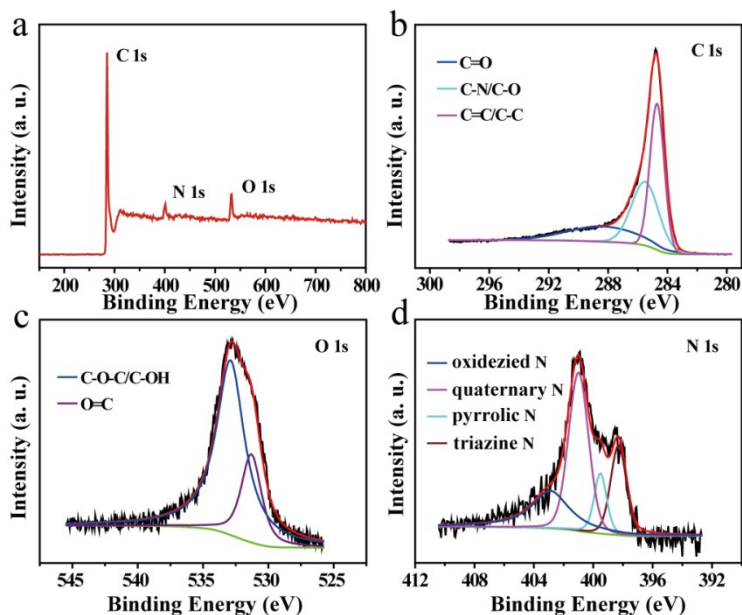
Fig. 10 XPS survey spectrum of Aa-NCa$_{850}$ (a); High-resolution XPS spectra of C 1s (b), O 1s (c) and N 1s (d) for Aa-NCa$_{850}$.
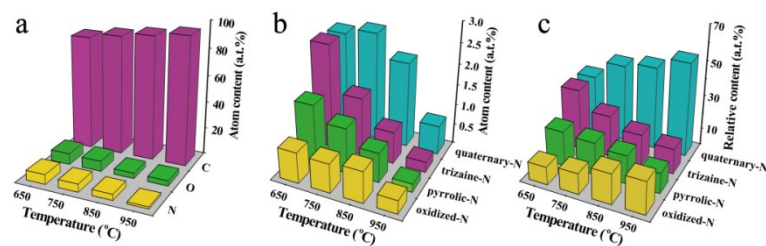
Fig. S11 Carbon, nitrogen and oxygen contents of Ta-NCa$_{650}$, Ta-NCa$_{750}$, Ta-NCa$_{850}$ and Ta-NCa$_{950}$ (a); The absolute content variations of oxidized N, graphitic N, pyrrolic N, and triazine N in Ta-NCa$_{650}$, Ta-NCa$_{750}$, Ta-NCa$_{850}$ and Ta-NCa$_{950}$ (b); The relative content variations of oxidized N, graphitic N, pyrrolic N, and triazine N in Ta-NCa$_{650}$, Ta-NCa$_{750}$, Ta-NCa$_{850}$ and Ta-NCa$_{950}$ (c).
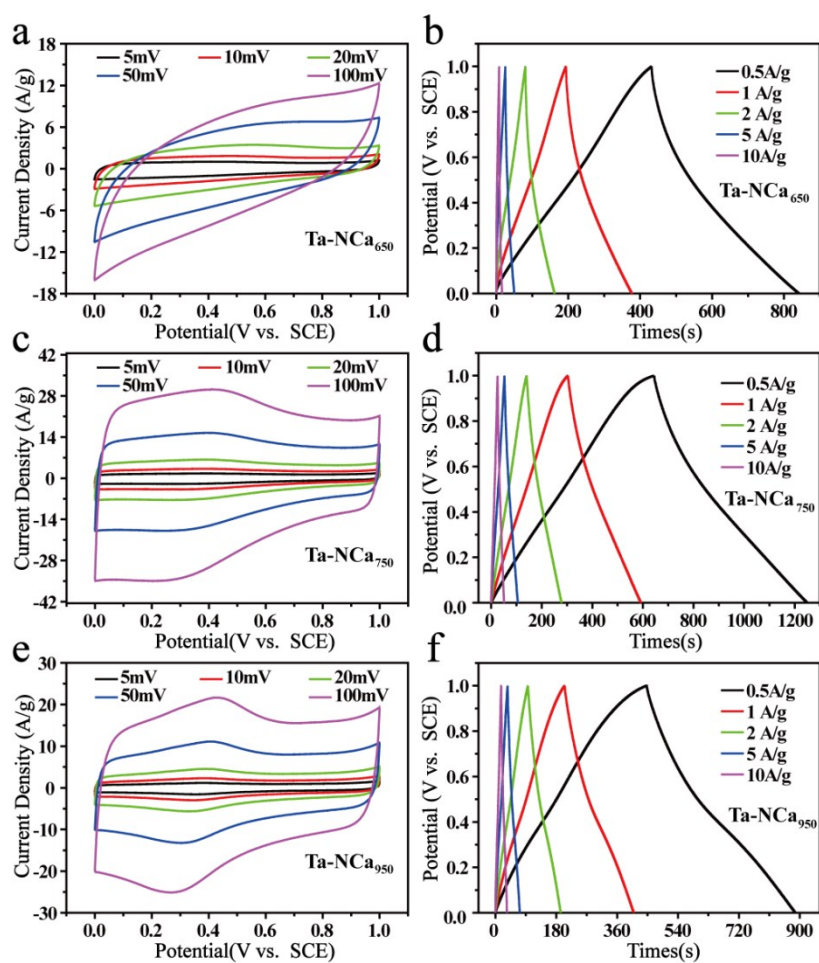
Fig. S12 Electrochemical performances of Ta-NCa$_{650}$, Ta-NCa$_{750}$ and Ta-NCa$_{950}$ in 1 M H$_2$SO$_4$. CV curves of Ta-NCa$_{650}$, Ta-NCa$_{750}$ and Ta-NCa$_{950}$ (e) at the scan rates from 5 to 100 mV s^{-1}; Galvanostatic charge discharge profiles of Ta-NCa$_{650}$, Ta-NCa$_{750}$ and Ta-NCa$_{950}$ (f) at the current densities from 0.5 to 10 A g^{-1}.
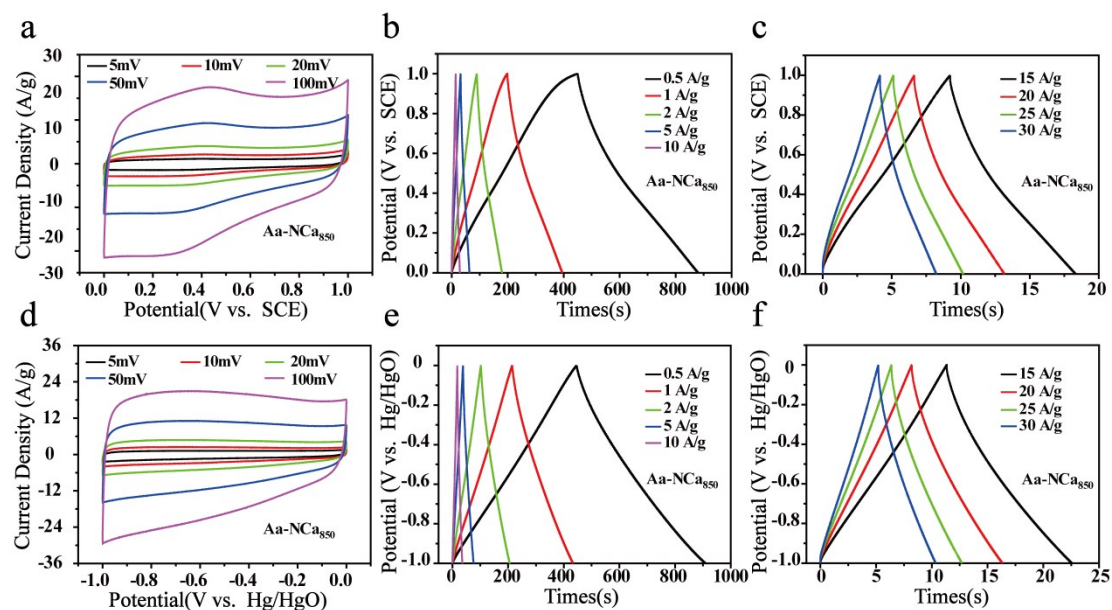
Fig. 13 CV curves of Aa-NCa$_{850}$ at the scan rates from 5 to 100 mV s^{-1} in 1 M H$_2$SO$_4$ (a); Galvanostatic charge discharge profiles of Aa-NCa$_{850}$ at the current densities from 0.5 to 30 A g^{-1} in 1 M H$_2$SO$_4$ (b and c); CV curves of Aa-NCa$_{850}$ at the scan rates from 5 to 100 mV s^{-1} in 6 M KOH (d); Galvanostatic charge discharge profiles of Aa-NCa$_{850}$ at the current densities from 0.5 to 30 A g^{-1} in 6 M KOH (e and f).

CV curves of Aa-NCa$_{850}$ display a quasi-rectangular shape and the CV curves keep almost unchanged with the increase of the scan rates from 5 to 100 mV s^{-1}. At a high current of 30 A g^{-1}, Ta-NCas have specific capacitances of 123 F g^{-1} in H$_2$SO$_4$ and 156 F g^{-1} in KOH.
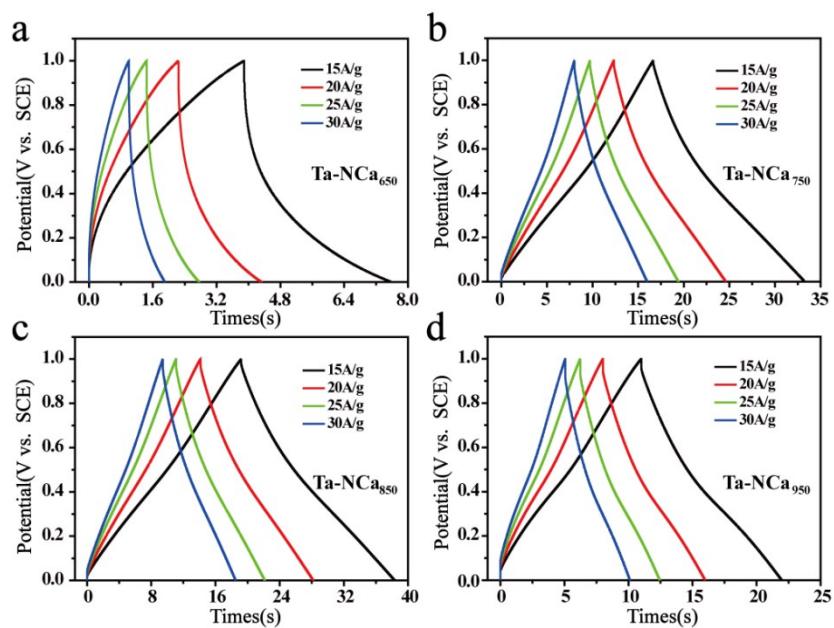
Fig. S14 Galvanostatic charge discharge profiles of Ta-NCa$_{650}$ (a), Ta-NCa$_{750}$ (b), Ta-NCa$_{850}$ (c) and Ta-NCa$_{950}$ (d) at the current densities from 15 to 30 A g^{-1} in 1 M H$_2$SO$_4$.
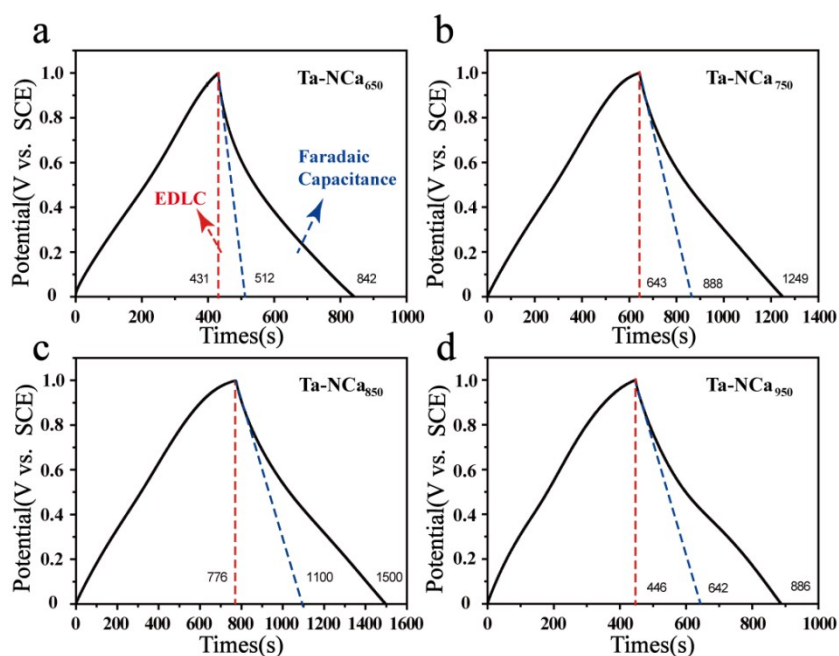
Fig. S15 Galvanostatic charge discharge profiles of Ta-NCa$_{650}$ (a), Ta-NCa$_{750}$ (b), Ta-NCa$_{850}$ (c) and Ta-NCa$_{950}$ (d) at 0.5 A g^{-1} in 1 M H$_2$SO$_4$ with the estimated EDLC and faradaic capacitance contributions being obtained from the discharge portions of differing slope.
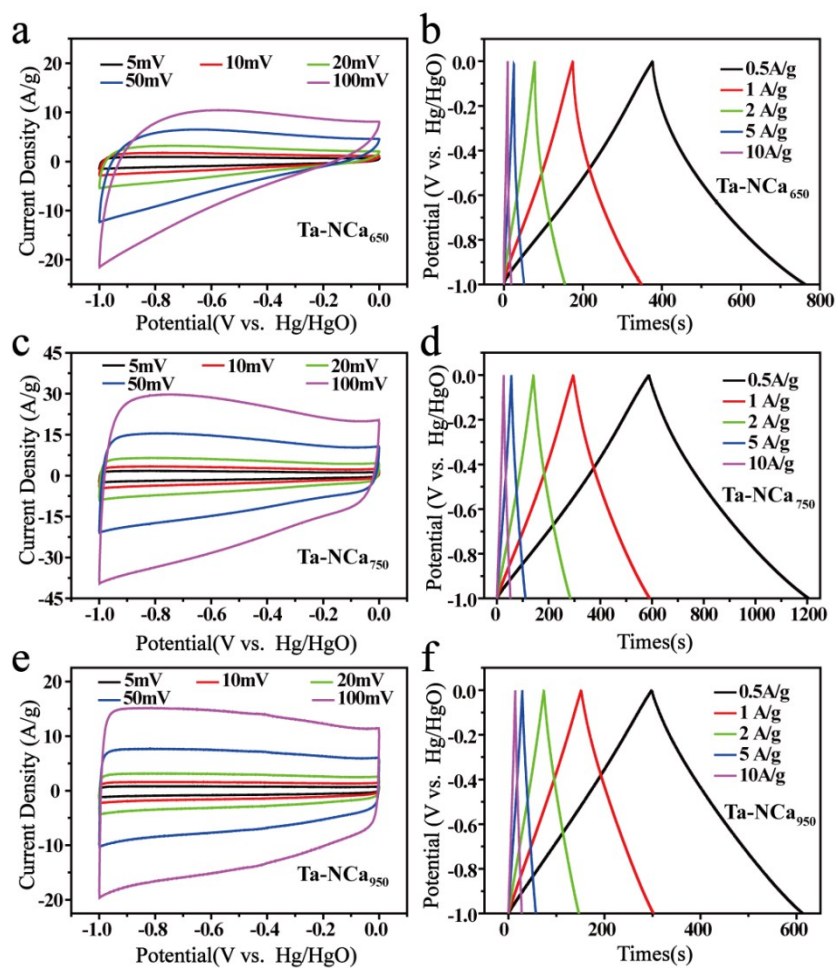
Fig. S16 Electrochemical performances of Ta-NCa$_{650}$, Ta-NCa$_{750}$ and Ta-NCa$_{950}$ in 6 M KOH. CV curves of Ta-NCa$_{650}$ (a), Ta-NCa$_{750}$ (c) and Ta-NCa$_{950}$ (e) at the scan rates from 5 to 100 mV s^{-1}; Galvanostatic charge discharge profiles of Ta-NCa$_{650}$ (b), Ta-NCa$_{750}$ (d) and Ta-NCa$_{950}$ (f) at the current density from 0.5 to 10 A g^{-1}.
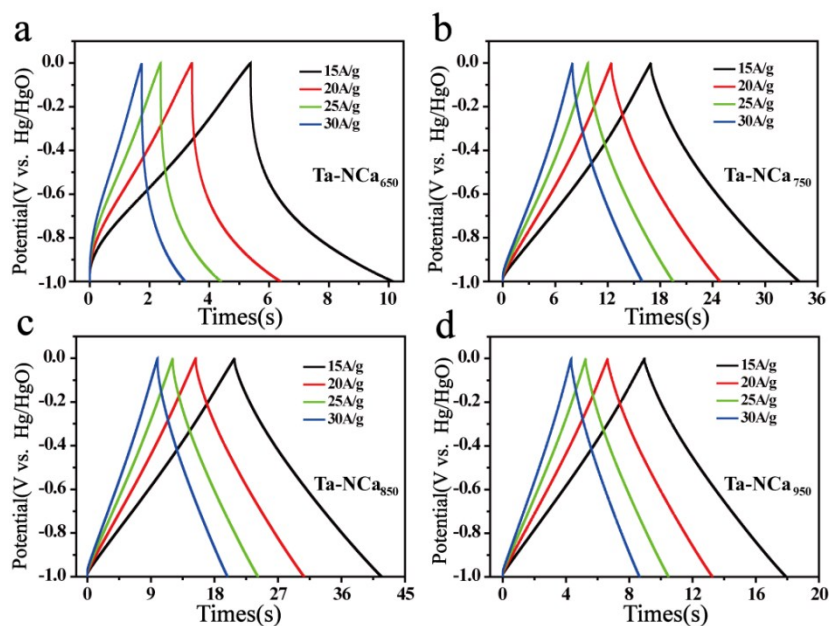
Fig. S17 Galvanostatic charge discharge profiles of Ta-NCa$_{650}$ (a), Ta-NCa$_{750}$ (b), Ta-NCa$_{850}$ (c) and Ta-NCa$_{950}$ (d) at the current densities from 15 to 30 A g^{-1} in 6 M KOH.
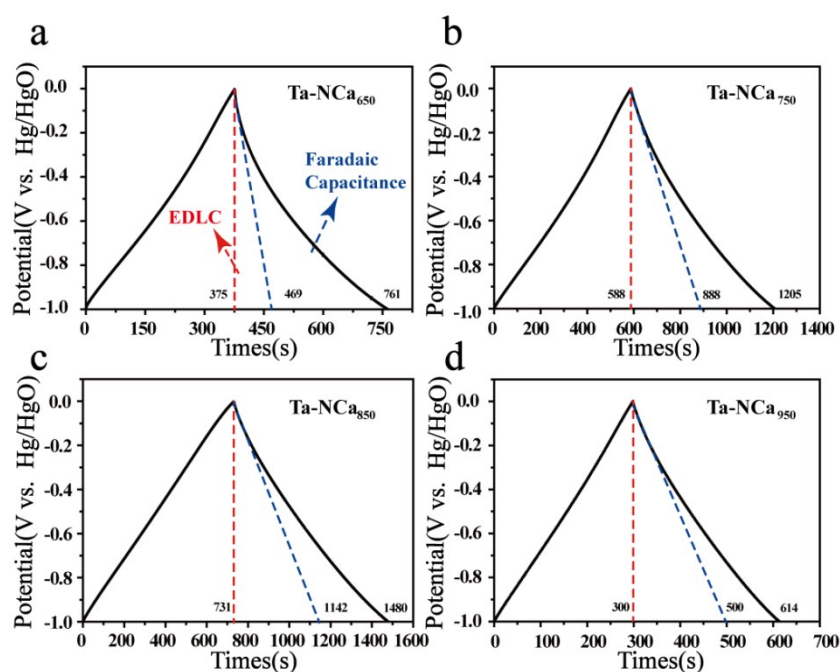
Fig. S18 Galvanostatic charge discharge profiles of Ta-NCa$_{650}$ (a), Ta-NCa$_{750}$ (b), Ta-NCa$_{850}$ (c) and Ta-NCa$_{950}$ (d) at 0.5 A g^{-1} in 6 M KOH with the estimated EDLC and faradaic capacitance contributions being obtained from the discharge portions of differing slope.
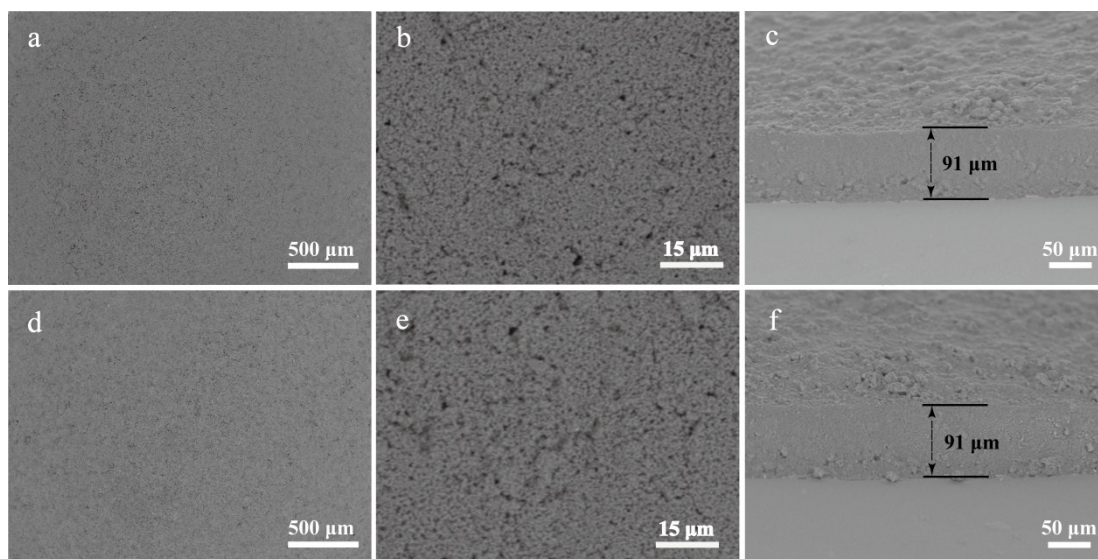
Fig. S19 SEM images of the working electrode film: surface (a, b) and cross section (c) before

5000 cycles, surface (d, e) and cross section (f) after 5000 cycles.

The thickness of the working electrode film is about 91 μm. No obvious morphology or thickness change can be observed to the working electrode film after 5000 cycles.
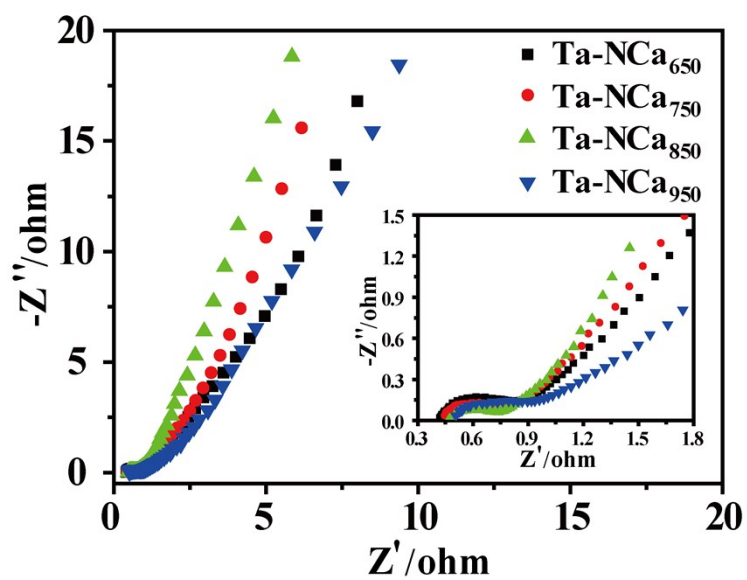
Fig. S20 Nyquist plots of Ta-NCas, The inset is magnified higher frequency region.
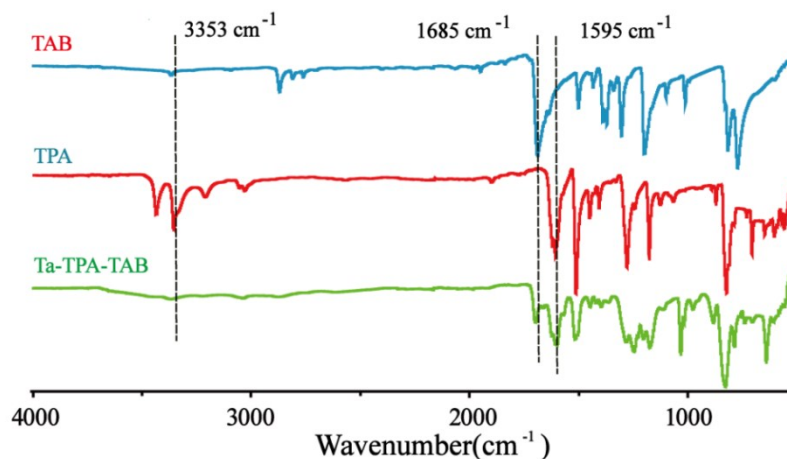
Fig. S21 FT-IR spectra of TPA, TAB, Ta-TPA-TAB.

In the FT-IR spectrum of Ta-TPA-TAB, characteristic peak at ~3320 cm^{-1} derived from N-H as well as the peak at 1686 cm^{-1} derived from C=O attenuates greatly, while absorption peak at 1578 cm^{-1} (C=N) appears, providing strong evidence for the successful synthesis of Schiff-base polymer Ta-TPA-TAB.
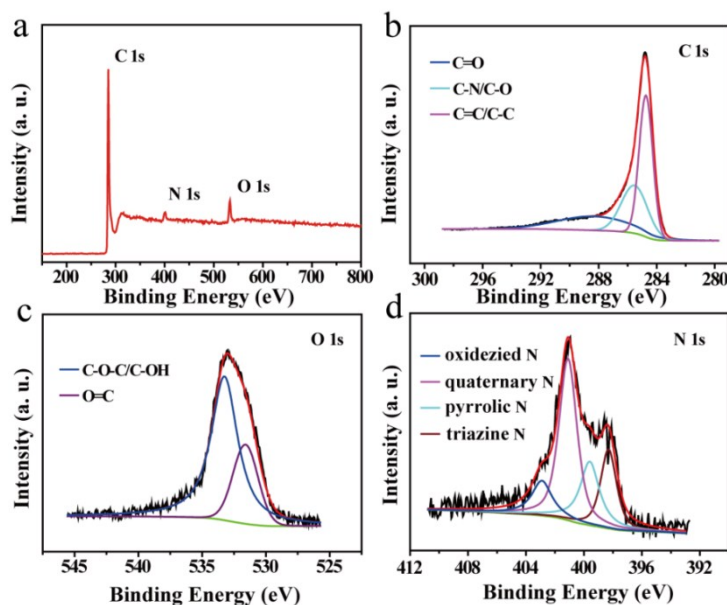
Fig. S22 XPS survey spectrum of Ta-NCb$_{850}$ (a); high-resolution XPS spectra of C 1s (b), O 1s (c) and N 1s (d) for Ta-NCb$_{850}$.

The XPS spectra of Ta-NCb$_{850}$ is similar to that of Ta-NCa$_{850}$ (Figure 3a-d) and corresponding analysis is described in the main text.

Table S1 surface elemental composition (atomic %) of TAA, TPA and Ta-TPA-TAA.

Samples	Composition (a.t. %)		
	C	N	O
TAA	75.35	24.65	0
TPA	74.97	0	25.03
Ta-TPA-TAA	76.50	14.32	9.18

Table S2 Surface area, porosity, surface elemental composition (atomic %) of samples.

	S_{BET} [a]	S_{micro} [b]	V_{total} [c]	Composition (a.t. %) [d]		
	$m^2\,g^{-1}$	$m^2\,g^{-1}$	$cm^3\,g^{-1}$	C	N	O
Ta-NCa$_{650}$	373	332	0.24	84.50	7.26	8.24
Ta-NCa$_{750}$	440	414	0.29	88.45	5.90	7.64
Ta-NCa$_{850}$	706	654	0.44	91.59	4.39	4.02
Ta-NCa$_{950}$	950	802	0.54	94.67	1.51	3.82
Aa-NCa$_{850}$	722	715	0.40	91.07	3.85	5.08
Ta-NCb$_{850}$	896	775	0.51	90.9	3.74	5.36

[a] Specific surface area obtained from BET. [b] Surface area of micropores calculated by the t-plot method. [c] Total pore volume. [d] Atomic percent of elements obtained from XPS analysis.

Table S3 Heteroatoms dopedcarbons as electrode materials of supercapacitors.

Electrode Materials	Electrolyte	Capacitance ($F g^{-1}$)	Current Density	Ref.
Ta-NCa$_{850}$	6 M KOH	374.5	0.5 A g^{-1}	This work
	1 M H$_2$SO$_4$	362	0.5 A g^{-1}	
TCNQ-CTF-800	1 M KOH	383	0.2 A g^{-1}	5
PMC-650	1 M H$_2$SO$_4$	312	0.5 A g^{-1}	6
HFAC-2	1 M KOH	525	0.25 A g^{-1}	7
	1 M H$_2$SO$_4$	556	0.25 A g^{-1}	
ABF-9%M	6 M KOH	289	0.5 A g^{-1}	11
TNNs-550	1 M H$_2$SO$_4$	298	0.2 A g^{-1}	13
N-MCS-200	6 M KOH	292	1 A g^{-1}	28
aNMC-0.5	1 M H$_2$SO$_4$	328	0.5 A g^{-1}	33
TC	6 M KOH	286.6	0.5 A g^{-1}	34
N/S-HCS	6 M KOH	280	1 A g^{-1}	35
G/CNTs-200	6 M KOH	202	0.5 A g^{-1}	46